Extended Discounting Scheme for Evidential Reasoning as Applied to MS Lesion Detection

Hongwei Zhu
Dept. of Systems Design Engineering
University of Waterloo
200 University Ave. W., Waterloo, ON, N2L 3G1
Canada
h4zhu@engmail.uwaterloo.ca

Otman Basir
Dept. of Systems Design Engineering
University of Waterloo
200 University Ave. W., Waterloo, ON, N2L 3G1
Canada
obasir@uwaterloo.ca

Abstract – *This paper extends a conventional discounting scheme commonly used with the Dempster-Shafer evidential reasoning to deal with conflict. The extended discounting scheme is able to augment, discount, and oppose existing evidence structures when discounting factors take values in different ranges. To show its effectiveness, the scheme is employed for detecting multiple sclerosis (MS) lesions based on multi-modality MR images. The approach is fully automated and unsupervised. Experimental results have demonstrated that in addition to the superior segmentation accuracies of brain tissues, good MS detection performances have been obtained (MS detection accuracy* 90.28%*, similarity index* 84.19%*, and sensitivity* 78.68% *on average).*

Keywords: Dempster-Shafer evidence theory, discounting, adaptive fuzzy evidential reasoning, brain tissue segmentation, MS detection.

1 Introduction

MR image segmentation is well known as an important step in volume analysis, visualization of regions of interest (ROI), and diagnosis of brain diseases. Multiple sclerosis (MS) lesion is one of the main signs of various degenerative brain diseases, and it primarily affects white matter (WM) of the central nervous system [1, 2]. It is believed that a good understanding of the size, number and spatial distribution of MS lesions may provide important clues, for monitoring their change over time, evaluating the corresponding diseases, and supporting diagnosis decisions.

Effectively segmenting brain MR images into three main tissues: white matter (WM), gray matter (GM), and cerebrospinal fluid (CSF), is a hard problem due to the existence of image noise, partial volume effects, the presence of smoothly varying intensity inhomogeneity, and large amounts of data to be processed. To handle these difficulties, a large number of approaches have been studied, including fuzzy logic methods [3], neural networks [2], Markov random field methods with the maximum expectation [1], statistical methods [4], and data fusion methods [5]. Different image analysis techniques have been studied for MS lesion detection, such as intensity based or model based, 2-D based or 3-D based, pyramidal and hierarchical techniques [1, 6, 9]. In [6], a region based algorithm is proposed on T1 images to segment brain tissues into WM, GM, CSF and MS. It is found that the validation of the white matter lesions is very difficult due to the similarity and junctions between MS lesions and gray matter. In [2], based on some crucial assumptions, the thresholding technique is first used to detect and contour all hyperintense regions, and partial elimination of artifacts is carried out using assumptions on sizes and shapes of MS and artifacts; final removal of artifacts is achieved by means of a neural network. In contrast to the above approaches, a model-based fully automated algorithm is presented in [1], for segmenting multi-modality MR images, where MS lesions are treated as outliers.

It is well recognized that the Dempster-Shafer evidence theory (DSET) is able to model uncertainty, and deal with imprecision and conflict [10]. To take advantage of this property, a DSET based data fusion scheme is proposed in this paper for MS lesion detection. First, a discounting scheme which is commonly used in DSET to deal with conflict of sources is extended. As a result, the extended discounting is able to augment, discount, or oppose existing evidence as required. Secondly, for MS lesion detection initial MS lesions are detected as outliers by employing the knowledge about the pixel intensities of brain tissues and MS lesions, during an adaptive fuzzy evidential reasoning (adaptive FDS for short) process. Adaptive FDS is developed for segmenting normal brain tissues in terms of WM, GM, CSF, based on multi-modality MR images (T1, T2 and PD) [7]. A further postprocess is developed to expand initial MS lesions through a DSET based relabelling of neighboring pixels, by taking advantage of the fact that most MS lesions are white matter lesions [1, 8, 9]. An evidence structure is constructed for each modality based on the distance between the investigated pixel intensity and prototypes of expected classes. To accommodate the distribution nature of pixel intensities within considered classes, the extended discounting scheme is employed. Evidence structures after adjustment by the extended discounting are further combined by the Dempster's rule, and decisions are obtained finally by the maximum commonality decision rule (MCD). To examine the effectiveness of the proposed approach, experiments are carried out on the abnormal data set (with MS lesions), which is obtained from the Simulated Brain Database (SBD) [11]. In addition to the high overall segmentation accuracies of normal brain tissues, good MS detection performances are obtained, in terms of MS detection

accuracy, similarity index, and sensitivity.

The remainder of this paper is organized as follows. The Dempster-Shafer evidence theory (DSET) is briefly reviewed in Section 2, and an extension of a commonly used discounting scheme is detailed in Section 3. Further, the brain tissue segmentation and MS detection scheme are outlined in Section 4, with emphasis on MS detection. Experimental results are provided in Section 5, and conclusions are finally presented in Section 6.

2 Review of Dempster-Shafer evidence theory

The Dempster-Shafer evidence theory manages uncertainty and imprecision in three levels [10]: representing evidence by focal elements and masses (basic probability assignments), combing evidence by the Dempster rule of combination, and making decisions by certain decision rules.

Let $\Omega = \{\omega_1, \cdots, \omega_c\}$ be a frame of discernment. 2^Ω is the power set composed of all possible subsets of Ω. Classes in Ω are assumed to be mutually exclusive and exhaustive. A function $m : 2^\Omega \rightarrow [0, 1]$ is called a *mass function*, if

$$\sum_{A \subseteq \Omega} m(A) = 1, \text{and } m(\emptyset) = 0 \tag{1}$$

Subset A with non-zero mass is called a *focal element* (focal for short). Focal elements and their masses form an *evidence structure*, expressed in the form: $\{(A, m(A))|A \subseteq \Omega, m(A) > 0\}$. $(A, m(A))$ is referred to as a piece of evidence. The value of $m(A)$ represents the degree of evidential support with which a specific element of Ω belongs to the exact set A, not to the subsets of A. Some common evidential measures are belief, plausibility and commonality, as defined below respectively (where $B \subseteq \Omega, A \subseteq \Omega, A \neq \emptyset$):

$$\begin{aligned} \textit{belief}: &\quad \text{Bel}(A) = \sum_{B \subseteq A} m(B) \\ \textit{plausibility}: &\quad \text{Pl}(A) = \sum_{B \cap A \neq \emptyset} m(B), \quad \text{Pl}(\emptyset) = 0 \\ \textit{commonality:} &\quad Q(A) = \sum_{A \subseteq B} m(B) \end{aligned}$$

The *Dempster's rule* combines independent evidence by:

$$\oplus_{i=1}^n m_i(A) = \begin{cases} K \sum\limits_{\cap_{i=1}^n A^i = A} \prod\limits_{i=1}^n m_i(A^i), & \text{if} A \neq \phi \\ 0, & \text{if} A = \phi \end{cases}$$

$$\text{with } K = \frac{1}{1-k}, \text{ and } \quad k = \sum_{\cap_{i=1}^n A^i = \emptyset} \prod_{i=1}^n m_i(A^i)$$

where $\oplus$ denotes the combination operator. A^i designates the focal in source i, and $m_i(A^i)$ is the corresponding mass. $\cap_{i=1}^n A^i$ denotes the intersection of focals A^1 through A^n. k can be interpreted as a measure of conflict among the sources to be combined. After the combination, a decision can be made by simply choosing the class with the maximum Bel, Pl, or Q.

3 An extended discounting scheme

To handle conflict of information sources, a discounting scheme has been introduced in DSET such that $\text{Bel}(A) = (1-\alpha) \times \text{Bel}(A)$, $\forall A \subset \Omega$, and $\text{Bel}(\Omega) = 1$. Correspondingly, mass functions are often modified in the following manner [10, 12–14]:

$$m^\alpha(A) = \begin{cases} (1-\alpha) \times m(A), & \text{if } A \subset \Omega \\ \alpha + (1-\alpha) \times m(\Omega), & \text{if } A = \Omega \end{cases} \tag{2}$$

where $\alpha \in [0, 1]$ is a discounting factor, and $m^\alpha(A)$ denotes the discounted mass of $m(A)$. The larger is α, the more masses are discounted from non frame of discernment focals, while the more mass is assigned to the frame of discernment Ω.

We now extend the above discounting scheme by allowing α out of range $[0, 1]$. The basic idea is that a discounting factor is viewed as an opinion to an existing evidence structure, and the extended discounting is allowed to augment, discount, or oppose the existing evidence structure according to the value of the discounting factor. The scenarios associated with this idea can be often found in the multi-evidence pooling systems, where decisions are made based on a set of existing evidence and the corresponding confidence (or evaluation) on these evidence. Evidence and corresponding confidence may be elicited in different manners, e.g., drawn by different experts, or based on different viewpoints.

Recall that in conventional discounting scheme given in Eq. (2), the masses of focal elements other than the frame of discernment Ω are scaled down by a non-zero discounting factor and the deducted masses are added to that of Ω. Taking a similar strategy, an augmenting process seems also straightforward by scaling up the masses of non Ω focals through taking masses away from $m(\Omega)$ if $m(\Omega) \neq 0$. This can be easily achieved by Eq. (2) also but with $\alpha < 0$, which is rewritten as

$$m^\alpha(A) = \begin{cases} (1-\alpha) \times m(A), & \text{if } A \subset \Omega \\ \alpha + (1-\alpha) \times m(\Omega), & \text{if } A = \Omega \end{cases} \tag{3}$$

$$\text{with} \qquad \frac{-m(\Omega)}{1-m(\Omega)} < \alpha < 0$$

where the later formula guarantees that $m^\alpha(A) \leq 1$ if $A \subset \Omega$, and $m^\alpha(A) \geq 0$ if $A = \Omega$, so that the augmented evidence structure still satisfies Eq. (1). This indicates that the maximum degree of augmenting is constrained by the mass of Ω in the investigated evidence structure.

For opposing an existing evidence structure, a discounting factor $\alpha > 1$ is able to attain this goal, since a negative value of $(1-\alpha) \times m(A)$ in Eq. (2) may be conceptually reasonable to be interpreted as an objection to the evidence associated with focal A while its complement $\bar{A} = \Omega - A$ is favored to a positive degree of $(\alpha - 1) \times m(A)$. In view of this, the discounting scheme in Eq. (2) with $\alpha > 1$ can be substituted by a new evidence structure:

$$\begin{aligned} m^\alpha(\bar{A}) &= (\alpha - 1) \times m(A), \text{ if } A \subset \Omega \\ m^\alpha(\Omega) &= 2 - \alpha + (\alpha - 1) \times m(\Omega) \\ \text{with} \quad 1 < \alpha &< \frac{1}{1-m(\Omega)} + 1 \end{aligned} \tag{4}$$

where the last formula ensures that the new mass m^{α} ranges in $[0, 1]$. It is trivial to show that the new evidence structure satisfies Eq. (1) also.

Recall that the discounting scheme is originally based on a statistical point of view [10]. As a matter of fact, the determination of masses has been extended beyond the statistical scope, and they can be associated with any other confidence measures, e.g., human subjective judgements. In view of this, a discounting factor can be of also other than the conventional statistical sense. Therefore, it would be more reasonable to view an extended discounting factor as a general evidence adjustment factor.

4 Application to MS detection

4.1 Overview

Three modality MR images, namely, T1, T2 and PD are treated as distinct information sources. The brain tissue segmentation and MS lesion detection are performed by a cascading hybrid process, as depicted in Fig. 1 (a). In this figure ESCU stands for the evidence structure construction unit. Figure 1 (b) depicts this unit. MF stands for membership function, and FS stands for a fuzzy evidence structure [7]. In Fig. 1 (b), PDES is refers to as the Proportional Difference Evidence Structure scheme, which is similar to the possibility distribution to mass function conversion scheme suggested in [16]. For details of PDES, please refer to [15]. FIS stands for fuzzy inferencing systems.

For "cascading", we refer to that three stages are involved sequentially: 1) stage 1, K-mean clustering applied to individual modalities, 2) stage 2, knowledge based MS initial detection and adaptive fuzzy evidential reasoning for brain tissue segmentation, 3) stage 3, Dempster-Shafer evidential reasoning involved postprocessing. In term of "hybrid", several techniques are involved (K-mean clustering, adaptive fuzzy evidential reasoning, Dempster-Shafer evidential reasoning, fuzzy inferencing), and the knowledge of characteristics of WM, GM, CSF, MS in distinct modalities is taken into consideration while MS lesions are detected as outliers. It is noticed that preprocessing required for extracting regions of interest (ROI) is skipped by virtual of ground truth images. Only the initial MS detection in stage 2 and the postprocessing in stage 3 are detailed in this paper. For details of adaptive fuzzy evidential reasoning, please refer to [7]. For an overall picture of the proposed approach, necessary parts are outlined below.

As usual, domain knowledge is required. The following knowledge is employed for brain tissue segmentation and MS detection:

K1: CSF is dark, GM is of medial intensities, and WM is bright in T1 image;

K2: CSF is bright, GM is of medial intensities, and WM is dark in both T2 and PD images;

K3: MS has almost similar pixel intensities as GM in T1 image;

K4: MS has almost similar pixel intensities as CSF respectively in T2 and PD images;

K5: MS often contacts WM.

Knowledge K1 through K4 is quite obvious when the three modality MR images are compared with corresponding ground truth images in Fig. 2, where only the ROI of brain composed of WM, GM, CSF, and MS is presented and all the others are expressed as dark background. Regarding knowledge K5, a very high percentage of MS lesions (around $90\% - 95\%$ of total MS lesions) are white matter lesions which occur within white matters and/or contact WM [1, 8, 9]. MS lesions inside CSF are not considered in this study.

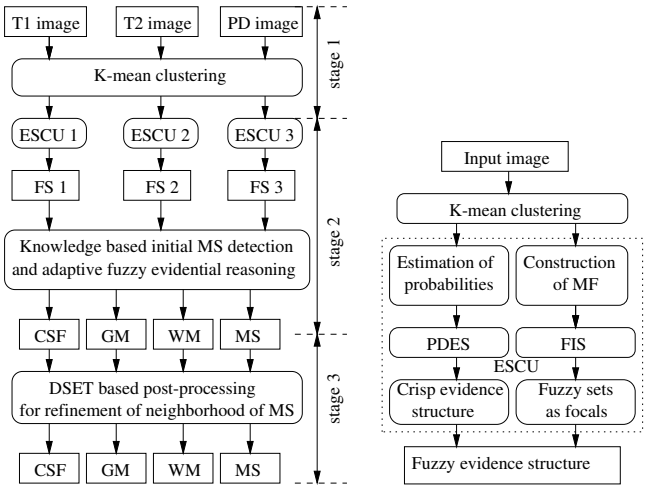

(a) The overall paradigm (b) ESCU

Fig. 1: Block diagram.

Within an ESCU, the K-mean algorithm is employed to cluster pixel intensities of ROI into 3 clusters for a given modality MR image. The number of clusters is set to 3. This is due to the indistinguishability between MS and one of normal brain tissues as indicated by K3 and K4. To handle this issue, compound classes are formulated, respectively depending on the modality investigated. Each resultant cluster is thus associated with one of the following classes: CSF, $\{$GM, MS$\}$, and WM for T1 images due to K3, $\{$CSF, MS$\}$, GM, and WM for T2 and PD images because of K4. Furthermore, these classes are used for establishing probabilistic evidence and fuzzy evidence, which are required by the adaptive fuzzy evidential reasoning [7].

4.2 Combining evidence for initial MS detection

To make use of the adaptive fuzzy evidential reasoning scheme (adaptive FDS) presented in [7], it is required that all information sources provide an identical set of component classes. However, as aforementioned, when brain MR images are abnormal (containing MS lesions), obtained evidence structures have different component classes. To handle this issue, given a pixel it is first examined whether it is MS using rules which are specified below. Such obtained MS pixels are referred to as initial MS lesions. If the pixel is not MS, associated with this pixel there is an identical set of component classes: CSF, GM, and WM for every modality, and adaptive FDS is then employed for labelling this pixel as one of normal brain tissues [7].

Let x_1, x_2, and x_3 be respectively the pixel intensity in T1, T2, and PD MR images, and let "$\in$" denote "is labelled

to". Initial MS pixels are detected by aggregating partial results through following rules.

R1: If $x_1 \in \{\text{GM, MS}\}$, $x_2 \in \{\text{CSF, MS}\}$, and $x_3 \in \{\text{CSF, MS}\}$, then the pixel is MS;

R2: If $x_1 \in \{\text{WM}\}$, $x_2 \in \{\text{CSF, MS}\}$, and $x_3 \in \{\text{CSF, MS}\}$, then the pixel is MS;

R3: If $x_1 \in \{\text{WM}\}$, $x_2 \in \{\text{GM}\}$, and $x_3 \in \{\text{CSF, MS}\}$, then the pixel is possible MS;

R4: If $x_1 \in \{\text{WM}\}$, $x_2 \in \{\text{CSF, MS}\}$, and $x_3 \in \{\text{GM}\}$, then the pixel is possible MS;

R5: If a pixel is possible MS and there exists MS in its 5×5 neighboring area, then the pixel is MS;

R6: If a pixel is possible MS, but there exists no MS in its 5×5 neighboring area, then the pixel is assigned to the brain tissue resulted from adaptive FDS.

The partial results in antecedents of rules R1 through R4 are obtained either by single-modality based K-mean clustering or by the maximum commonality decision rule (MCD) on the derived evidence structures of corresponding modalities (in adaptive FDS a fuzzy evidence structure is constructed for a given pixel from each modality). Rules R1 and R2 are directly associated with knowledge K3 and K4 presented in Section 4.1. R5 and R6 make use of the spatial similarity between neighboring pixels since MS pixels often tend to form regions of certain sizes.

4.3 Post-processing

Further postprocessing is employed to refine the labels of the neighboring GM and WM pixels surrounding the initial MS lesions by the DSET based reasoning and using domain knowledge. As a consequence of the adaptive fuzzy evidential reasoning and the initial MS detection, each pixel in ROI is categorized into one of 4 classes: WM, GM, CSF, and MS. Using knowledge K5 in Section 4.1, a screening process is first performed such that if an initial obtained MS pixel is not adjacent to WM, it is recovered to one of the normal brain tissues: WM, GM, and CSF, whatever is obtained by adaptive FDS. Secondly, initial MS regions are formed by grouping the surviving MS pixels after the screening process, which are spatially adjacent either directly or indirectly. Two MS pixels are considered adjacent directly if one is located in the 8-neighborhood area of the other; Two MS pixels which are not adjacent directly are considered adjacent indirectly if their neighboring MS pixels are either directly or indirectly adjacent. Furthermore, for each of MS regions, its mean pixel intensity is computed. After these two steps, an iterative process is carried out for relabelling the surrounding WM and GM pixels of each MS region by the DSET based reasoning with the extended discounting scheme.

Given a MS region R_i in modality i, let B_i be a queue containing the neighboring WM and GM pixels of R_i that have not yet been visited (processed in the iterative procedure). Let $\overline{\text{MS}}_i$ be the mean pixel intensity of R_i, and $\overline{\text{WM}}_i$ the mean WM pixel intensity of modality i for the labelled WM by adaptive FDS. The refinement is realized through the following three-step iterative process.

- Step 1: Construct an evidence structure ES_i for a pixel in B_i if B_i is not empty, where $i = 1, 2, 3$. Like common distance based clustering approaches, such as K-mean and fuzzy C-mean methods, the distances of x_i to the two prototypes of MS and WM, in terms of their mean pixel intensities, are employed to represent evidence. Notice that x_i segmented as GM by adaptive FDS is not considered for refinement when it contacts CSF and/or background regions through a GM region. By this treatment, only those GM pixels which are surrounded by MS and/or WM are considered for refinement. This means that the GM pixels which are surrounded by MS and/or WM will be refined to MS or WM. As far as evidence is concerned, the closer is a pixel intensity from a prototype, the more likely it belongs to the corresponding class. By referring to the membership values used in the fuzzy C-mean approach, we define the evidence, in terms of the degrees to which x_i belongs to class MS and WM, respectively by

$$\mu^i_{\text{MS}} = \frac{s^i}{\left(x_i - \overline{\text{MS}}_i\right)^2}, \quad \mu^i_{\text{WM}} = \frac{s^i}{\left(x_i - \overline{\text{WM}}_i\right)^2} \quad (5)$$
$$\text{with} \quad (s^i)^{-1} = \frac{1}{\left(x_i - \overline{\text{MS}}_i\right)^2} + \frac{1}{\left(x_i - \overline{\text{WM}}_i\right)^2}$$

Using the evidence structure building scheme developed in [7, 15], an evidence structure is constructed based on the above measures as follows,

If $\mu^i_{\text{MS}} > \mu^i_{\text{WM}}$, ES_i is

$$\left\{ \left(\{\text{MS}\}, \frac{\mu^i_{\text{MS}} - \mu^i_{\text{WM}}}{\mu^i_{\text{MS}}} \right), \left(\{\text{MS, WM}\}, \frac{\mu^i_{\text{WM}}}{\mu^i_{\text{MS}}} \right) \right\} \quad (6)$$

else if $\mu^i_{\text{MS}} < \mu^i_{\text{WM}}$, ES_i is

$$\left\{ \left(\{\text{WM}\}, \frac{\mu^i_{\text{WM}} - \mu^i_{\text{MS}}}{\mu^i_{\text{WM}}} \right), \left(\{\text{MS, WM}\}, \frac{\mu^i_{\text{MS}}}{\mu^i_{\text{WM}}} \right) \right\} \quad (7)$$

else $\text{ES}_i = \{(\{\text{MS, WM}\}, 1)\}$.

- Step 2: Discount evidence provided in Eq. (6) or (7) whatever is chosen. The constructed evidence structures in Step 1 take into consideration only distances of x_i from the prototypes of MS and of WM, without paying any attention to the nature of the distribution of pixel intensities inside the two classes MS and WM. As we know, it may be more likely that x_i belongs to a widely scattered class to whose prototype x_i has a larger distance rather than a dense class to whose prototype x_i has a smaller distance. To accommodate this fact, the extended discounting scheme described in Section 3 is utilized as follows. Notice that if the evidence structure constructed in Step 1 has the only focal element of the frame of discernment, it is not considered for discounting.

  For all $x_i \in R_i$, ratios of squared distances $\rho_i = (x_i - \overline{\text{WM}}_i)^2/(x_i - \overline{\text{MS}}_i)^2$ are calculated and sorted, and their medial value, say $\bar{\rho}_i$, is selected to serve as

a representative ratio of the squared distances between MS region R_i to WM protocol and that to MS protocol. The selection of the medial value of ratios ensures the representative less sensitive to noise. Furthermore, considering that a smaller size of MS lesion tends to produce a larger $\bar{\rho}_i$, $\bar{\rho}_i$ is thus upper bounded by a threshold τ in order to overcome this dominant effect. τ is empirically set to 2000 in later experiments. Using ratio ρ_i and medial ratio $\bar{\rho}_i$, an adjustment factor α^i (i.e., a broad-sense discounting factor) is determined for modality i as follows:

- if $\rho_i > 1$, let $\alpha_0^i = 1 - \frac{1-\bar{\rho}_i/\rho_i}{1-1/\rho_i}$, then
  - if $\bar{\rho}_i < 1$, augmenting with $\alpha^i = \max\{1 - \frac{1}{m(A)}, \alpha_0^i\}$
  - if $1 \leq \bar{\rho}_i \leq \rho_i$, discounting with $\alpha^i = \alpha_0^i$
  - if $\rho_i < \bar{\rho}_i$, opposing with $\alpha^i = \min_{A \subset \Omega}\{\frac{1}{m(A)} + 1, \alpha_0^i\}$
- if $\rho_i < 1$, let $\alpha_0^i = 1 - \frac{1-\rho_i/\bar{\rho}_i}{1-\rho_i}$, then
  - if $\frac{1}{\bar{\rho}_i} < 1$, augmenting with $\alpha^i = \max\{1 - \frac{1}{m(A)}, \alpha_0^i\}$
  - if $1 \leq \frac{1}{\bar{\rho}_i} \leq \frac{1}{\rho_i}$, discounting with $\alpha^i = \alpha_0^i$
  - if $\frac{1}{\rho_i} < \frac{1}{\bar{\rho}_i}$, opposing with $\alpha^i = \min_{A \subset \Omega}\{\frac{1}{m(A)} + 1, \alpha_0^i\}$
- if $\rho_i = 1$, $\alpha^i = 0$

where $m(A)$ denotes the mass of the singleton class set in the selected evidence structure of Eq. (6) or (7) by comparing μ^i_{MS} with μ^i_{WM} (i.e., comparing ρ_i with 1 equivalently). Therefore, a new discounted evidence structure is accordingly derived by Eq. (2), Eq. (3), or Eq. (4) meanwhile the above α^i (taking the place of α) meets the constrains required by these three types of extended discounting.

Now let us look at how the above extended discounting works by analyzing an example with $\rho_i > 1$ and $\bar{\rho}_i < 1$. Due to $\rho_i > 1$, an original evidence structure is constructed by Eq. (6):

$$m(A) = \begin{cases} \frac{(x_i - \overline{\text{WM}}_i)^2 - (x_i - \overline{\text{MS}}_i)^2}{(x_i - \overline{\text{WM}}_i)^2}, & \text{if } A = \{\text{MS}\} \\ \frac{(x_i - \overline{\text{MS}}_i)^2}{(x_i - \overline{\text{WM}}_i)^2}, & \text{if } A = \{\text{MS}, \text{WM}\} \end{cases}$$

and α_0^i is determined by $\alpha_0^i = 1 - \frac{1-\bar{\rho}_i/\rho_i}{1-1/\rho_i}$. Furthermore, due to $\bar{\rho}_i < 1$, α^i is determined by $\alpha^i = \max\{1 - \frac{1}{m(A)}, \alpha_0^i\}$, and the extended discounting is really augmenting (for $\alpha^i < 0$) which produces a new evidence structure by Eq. (3):

$$m^{\alpha^i}(A) = \begin{cases} \frac{(x_i - \overline{\text{WM}}_i)^2 - \bar{\rho}_i(x_i - \overline{\text{MS}}_i)^2}{(x_i - \overline{\text{WM}}_i)^2}, & \text{if } A = \{\text{MS}\} \\ \frac{\bar{\rho}_i(x_i - \overline{\text{MS}}_i)^2}{(x_i - \overline{\text{WM}}_i)^2}, & \text{if } A = \{\text{MS}, \text{WM}\} \end{cases}$$

Obviously, $m^{\alpha^i}(A)$ is larger than $m(A)$ for $A = \{\text{MS}\}$ since $\bar{\rho}_i < 1$. Thus the evidence is augmented really. Other cases with different combinations of ρ_i and $\bar{\rho}_i$ can be easily analyzed and verified similarly.

- Step 3: Combine the adjusted evidence structures of three modalities by the Dempster's rule, and relabel the neighboring MS or GM pixels by the maximum commonality decision rule (assigning the pixel to the class with the maximum commonality). If a pixel is reclassified to the MS class, add this pixel to R_i, then search and add to B_i its boundary WM and GM pixels if they have not yet been processed during the refinement process. Once a new pixel is added to B_i, $\overline{\text{MS}}_i$'s, for $i = 1, 2, 3$, are updated in an accumulated manner. But, the WM prototype is not modified considering the fact that the size of WM region is relatively large and the refinement of a small number of pixels has less impact on it. The refinement process terminates if B_i is empty; return to Step 1 otherwise.

After the accomplishment of the above iterative refinement process, a similar step as the previous screening process is carried out for removing those absolutely misclassified MS pixels using knowledge K5. Consequently, a MS region having no neighbor of WM is labelled to the neighboring class with which the suspected MS region has the longest boundary. The reason to redo this is due to the fact that the above relabelling may produce MS lesions which don't touch WM.

5 Experimental results

In this section, experiments are carried out on the abnormal brain MR image data set with multiple sclerosis lesions (MS), denoted by MS-SBD, which is obtained from the Simulated Brain Database (SBD), a benchmark developed by the McConnell Brain Imaging Centre [11]. In MS-SBD, T1, T2, PD images have been registered, and corresponding ground truth images are also available for evaluation. The adopted MR images are simulated as follows: the slice thickness is 1mm; the noise level is 3%; and the level of intensity non-uniformity is set to 20%. We carry out the experiment on a large number of slices for this data set, and results for 31 MR images from slice 80 to slice 110 in the axial direction are reported. These slices are located almost in the middle part along the axial axis, and have an appropriate portion for every normal brain tissue and a good number of MS lesions.

In addition to the overall segmentation accuracy $\mathcal{A}$, as computed by the ratio between the number of correctly segmented pixels and that of the entire pixels in the ROI (including WM, GM, CSF and MS), we are interested in examining the performance of MS detection. Four additional measures are employed, and they are MS detection accuracy $\mathcal{A}_{\text{MS}}$, the number of false alarms of MS lesions FA, similarity index SI, sensitivity SE.

MS detection accuracy $\mathcal{A}_{\text{MS}}$ refers to the ratio between the number of the correctly detected MS pixels and the total number of MS pixels given a slice. The number of false alarms FA refers to the number of misdetected MS lesions

which are originally normal brain tissues. Similarity Index is defined as

$$SI = \frac{2|S1 \cap S2|}{|S1| + |S2|}$$

where $S1$ and $S2$ stand for two segmentations to be compared [17], and $|.|$ denotes cardinality. For MS detection, $S1$ denotes MS pixels in a ground truth image, and $S2$ is detected MS pixels by the proposed approach. Therefore, $|S1|$ and $|S2|$ are respectively referred to as the number of the true MS pixels and that of the labelled MS pixels. $|S1 \cap S2|$ is the number of MS pixels correctly detected. In essence, similarity index SI measures the degree of the overlap of MS pixels between the labelled image and the ground truth image. SI attains the maximum value 1 if all MS pixels are detected correctly without any false alarms in the same time; SI is zero if no true MS pixel is detected at all. Sensitivity is defined by

$$SE = \frac{TP}{TP + FN}$$

where TP denotes true positive, the number of lesions detected correctly by an algorithm, and FN stands for false negative, the number of lesions missed by the algorithm [2]. Different from similarity index, sensitivity measures the performance from a viewpoint of MS lesions (regions composed of MS pixels), without considering sizes of MS lesions (the numbers of pixels within MS lesions).

Referring to the results on normal brain SBD data sets (without MS lesions) [7], we apply adaptive FDS with $\sigma = 1.0$ to MS-SBD, and perform further MS pixel detection by the method presented in Section 4. σ is a parameter involved in the determination of width of Gaussian kernel functions in the Parzen window technique required in adaptive FDS. Detailed results are shown in Fig. 3, in terms of slice-wise overall accuracy $\mathcal{A}$, MS detection accuracy $\mathcal{A}_{\text{MS}}$, similarity index SI, and sensitivity SE. They are also summarized in Table 1, in terms of the minimum, the average, and the maximum.

Fig. 3 shows that very high overall segmentation accuracies are obtained for the 31 slices, ranging from 95.34% to 97.09%. Fig. 3 shows also that performances of MS detection vary with slices. They are affected by several factors, such as indistinguishability between MS and normal brain tissues, sizes of MS lesions, and locations of MS lesions in ROI, etc. For visual evaluation of MS detection performance, MS-SBD images at three slices, their ground truth images, and segmentation results, are presented in Fig. 2, where row 1, 2, and 3 respectively correspond to slice 99, 93 and 110. In addition, both the true MS lesions (designated by True MS) and the detected MS lesions (designated by Det. MS) are presented. The MS lesions for slice 99 have relatively large sizes, but most of them are located in the boundary areas between WM and CSF. Our approach performs well for this slice, and all MS lesions are detected correctly since $SE = 1$ at slice=99 in Fig. 3 (d), but without resulting in exactly the same sizes and regions as the true ones (SI is around 88% at slice=99 in Fig. 3 (c)). Row 2 of Fig. 2 presents images for slice 93, which corresponds to the worst result with the minimum $\mathcal{A}_{\text{MS}}$ and the minimum SI. For this slice, out of 9 MS lesions, three are located in the highly mixed areas, which are adjacent to CSF, WM, and other classes represented by the dark pixels, while these MS lesions are of small sizes. Please see the central bright pixels of the zoomed region shown in Fig. 4 (d). As far as the three original modality images in Fig. 4 (a), (b) and (c) are concerned, these three MS lesions are really hard to recognize even by human visual inspection. In addition to the difficulty found in slice 93, row 3 of Fig. 2 shows also the difficulty of detecting large MS lesions which are located in confused boundary areas. However, the larger MS lesion that separates the big WM tissue into two parts and has low contrast with its neighboring normal tissues in both T1 and PD images is correctly detected by the algorithm.

Table 1: Summary of performance

	min	avg	max
$\mathcal{A}$	95.34	96.09	97.09
$\mathcal{A}_{\text{MS}}$	67.50	90.28	100.00
SI	67.92	84.19	95.15
SE	40.00	78.68	100.00
FA	0	1.03	4

Fig. 3 shows that the worst results of A_{MS} and SI happen at slice 93, while the worst SE happens at slice 92. Table 1 indicates that $\mathcal{A}_{\text{MS}}$ ranges from 67.5% to 100% with average 90.28%. The resultant SI is in the range from 67.92% to 95.15% and 84.19% on average. As stated in [17], similarity index is a derivation of kappa statistic, and $SI > 0.7$ indicates excellent agreement between the detected MS and the true MS according to [18]. In this sense, good overall MS detection performance is obtained by our approach. In terms of the sensitivity measure, SE is in the range from 40% to 100% and 78.68% on average. In terms of number of false alarms FA, the average is 1.03, which accounts for 18.71% of the average number of true MS lesions 5.51 for all the 31 slices. Out of the 31 slices, 11 slices have no false alarms, and the maximum number of false alarms per slice is 4.

In addition to the aforementioned difficulty in MS detection, another reason for the relatively low MS detection performance may be due to the reference ground truth images, which may not be a perfect reference though they have been obtained after the delicate considerations of experts. It is recognized that MS lesion assessment varies with human medical experts. For example, it is reported that the similarity index between two human experts is very low [1]. If we view the ground truth images as an expert's opinion, the obtained similarity indexes in the experiment are reasonably larger.

6 Conclusions

In this paper, for effectively making use of the Dempster-Shafer evidential reasoning we propose an extended discounting scheme, which is able to augment, discount, and oppose existing evidence structures. Experiments for multiple sclerosis (MS) lesion detection have justified that the extended discounting scheme associated Dempster-Shafer

evidential reasoning results in good MS detection performance.

It is believed that this extended discounting scheme is conceptually reasonable since the extended discounting is actually a general sense adjustment to existing evidence structures. This fits well the human judgment convention when evaluation is required for existing evidence. In the future work, the extended discounting scheme will be studied for other applications with more complicated evidence structures.

References

[1] K. Van Leemput, F. Maes, D. Vandermeulen, A. Colchester, and P. Suetens. Automated segmentation of multiple sclerosis lesions by model outlier detection. *IEEE Trans. Medical Imaging*, 20:677-688, 2001.

[2] D. Goldberg-Zimring, A. Achiron, and S. Miron. Automated detection and characterization of multiple sclerosis lesions in brain MR images. *Magnetic Resonance Imaging*, 16: 311-318, 1998.

[3] Y. Hata, S. Kobashi, and S. Hirano. Automated segmentation of human brain MR images aided by fuzzy information granulation and fuzzy inference. *IEEE Trans. SMC, Part C*, 30: 381-395, 2000.

[4] T.W. Kim and C.H. Paik. Unsupervised statistical adaptive segmentation of brain MR images using the MDL principle. In *Proc. 20th Annual Int. Conf. of the IEEE*, 2: 617-620, 1998.

[5] H. Zhu and O. Basir. Fuzzy evidential reasoning applied to multi-modality MR brain image segmentation with source selection. In *Proc. 7th Joint Conf. Info. Sci.*, 2003.

[6] S.A. Hojjatoleslami, F. Kruggel, and D.Y. von Cramon. Segmentation of white matter lesions from volumetric MR images. *Medical Image Computing and Computer-Assisted Intervention - MICCAI'99*, pages 52-61, 1999.

[7] H. Zhu and O. Basir. Adaptive fuzzy evidential reasoning for automated brain tissue segmentation. In *Proc. 7th Int. Conf. Information Fusion*, Stockholm, Sweden, 2004.

[8] K.R. Maravilla. Multiple sclerosis. In D.D. Stark, W.G. Bradley, editors, *Magnetic Resonance Imaging*, St. Louis, MO: Mosby, pages 344-358, 1988.

[9] M. Kamber, R. Shinghal, D.L. Collins, G.S. Francis, and A.C. Evans. Model-based 3-D segmentation of multiple sclerosis lesions in magnetic resonance brain images. *IEEE Trans. Medical Imaging*, 14: 442-453, 1995.

[10] G. Shafer, A Mathematical Theory of Evidence, Princeton University Press, Princeton, NJ, 1976.

[11] D.L. Collins, A.P. Zijdenbos, V. Kollokian, J.G. Sled, N.J. Kabani, C.J. Holmes, and A.C. Evans. Design and construction of a realistic digital brain phantom. *IEEE Trans. Medical Imaging*, 17: 463-468, 1998.

[12] P. Smets. Data fusion in transferable belief model. In *Proc. 3rd Int. Conf. Information Fusion*, pages 21-33, 2000.

[13] J.W. Guan and D.A. Bell. Approximate reasoning and evidence theory. *Information Sciences*, 96:207-235, 1997.

[14] S. Fabre, X. Briottet, and A. Appriou. Impact of contextual information integration on pixel fusion. *IEEE Trans. Geosci. Remote Sensing*, 40: 1997-2010, 2001.

[15] H. Zhu and O. Basir. A scheme for constructing evidence structures in Dempster-Shafer evidence theory for data fusion. In *Proc. 5th IEEE Int. Symposium on Computational Intelligence in Robotics and Automation*, pages 16-20, 2003.

[16] D. Dubois and H. Prade. On several representations of an uncertainty body of evidence. In M. M. Gupta, E. Sanchz, editors, *Fuzzy Informaton and Decision Processes*, pages 167-181, North-Holland, New-York, 1982.

[17] A.P. Zijdenbos, B.M. Dawant, R.A. Margolin, and A.C. Palmer. Morphometric analysis of white matter lesions in MR images: method and validation. *IEEE Trans. Medical Imaging*, 13: 716-724, 1994.

[18] J.J. Bartko. Measurement and reliability: statistical thinking considerations, *Schizophrenia Bullet.*, 17:483-489, 1991.

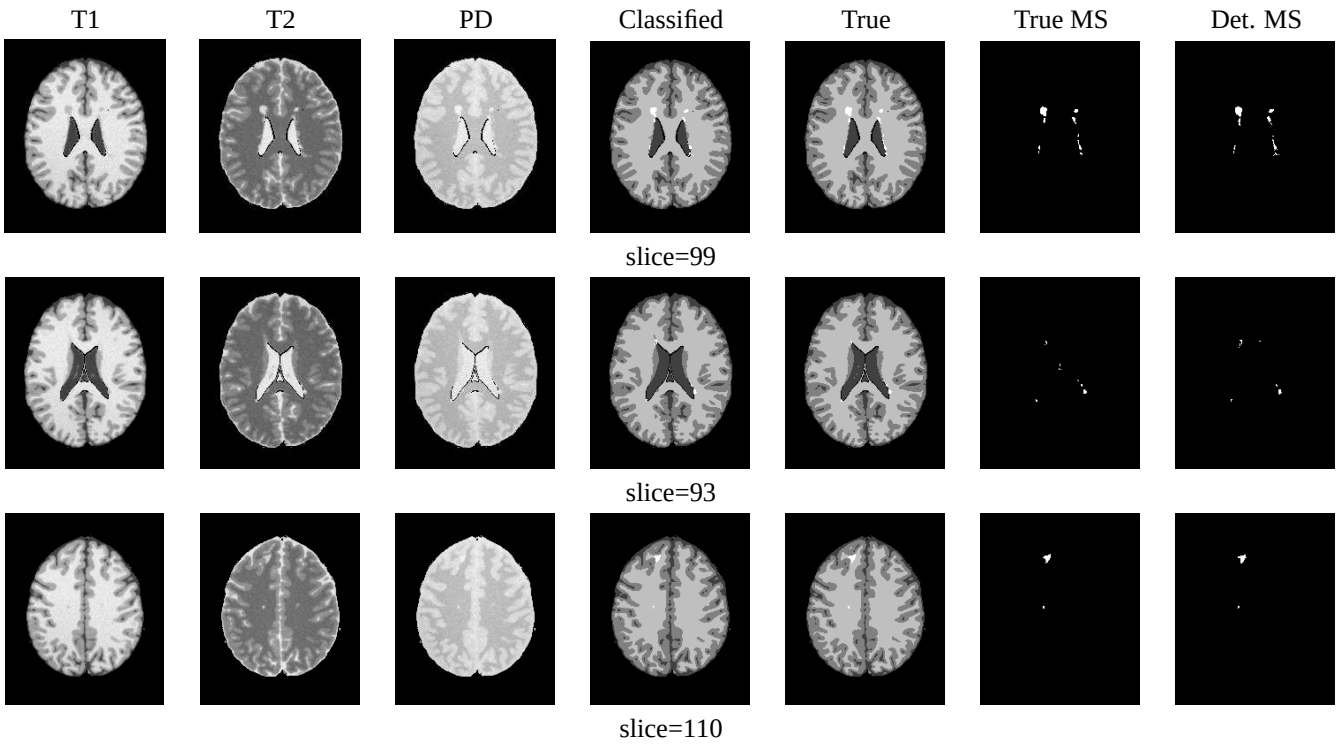

Fig. 2: Example MS-SBD images, and segmentation results.

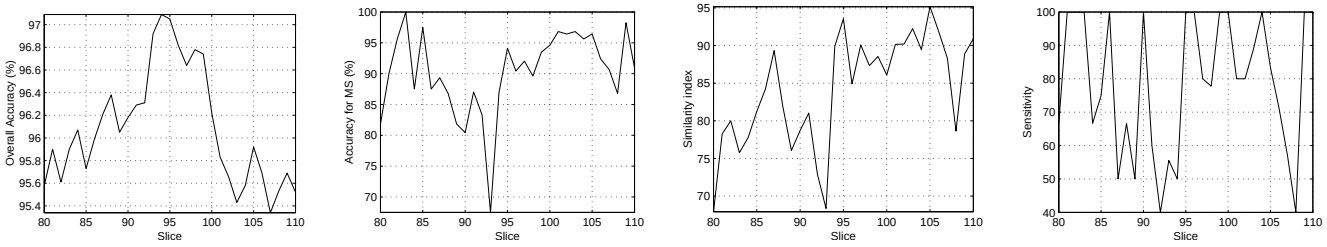

(a) $\mathcal{A}$ (b) $\mathcal{A}_{\text{MS}}$ (c) SI (d) SE

Fig. 3: Evaluation of performance.

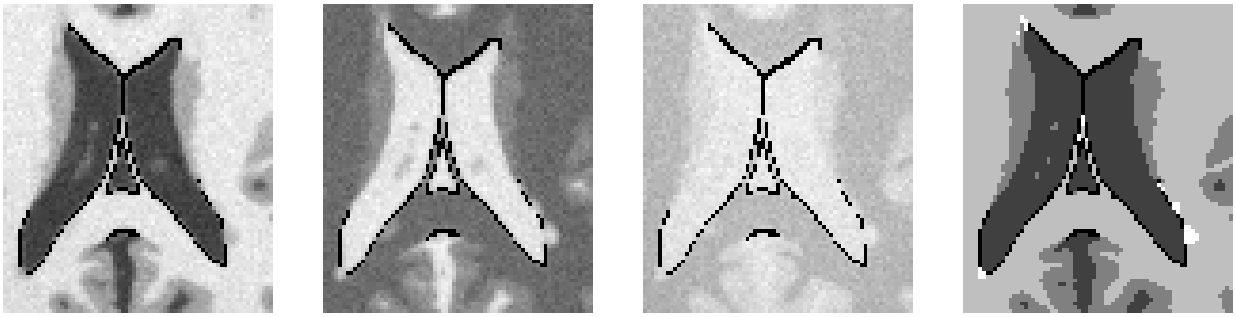

(a) T1 (b) T2 (c) PD (d) Ground truth

Fig. 4: Zoomed local regions, slice 93.